A Method of Suppressing Unbalance Vibration of AMBs Based on Flux Feedback Control

Wei Huang[*], Zhiquan Deng[*a], Cong Peng[*], Kexiang Li[*], Kaiwen Cai[*], Lei Mei[**]
[*]College of Automation Engineering, Nanjing University of Aeronautics and Astronautics, China
[**]College of Electrical Engineering and Control Science, Nanjing University of Technology, China
[*a]E-mail: dzq@nuaa.edu.cn

Abstract — In this paper, an unbalance vibration suppression method based on flux feedback control strategy is proposed. The air gap flux is obtained from an improved flux observer. The principle of generalized notch filter is analyzed in detail and the transmission matrix parameters are reasonably designed so that the system can keep stable in a wide speed range. The simulation results show that adding generalized notch filter algorithm into the control system can restrain the vibration force caused by the mass unbalance of rotor during rotation.

I. INTRODUCTION

Compared with the conventional bearings, magnetic bearings have been widely used in the high-speed motor, aerospace and other fields with no wear, no friction, no lubrication and other excellent characteristics [1-3]. Due to the limitation of material and machining level, there is unbalanced mass in the magnetic suspension rotor inevitably which results in the periodic fluctuations of the displacement signal when the rotor rotates [4][5]. Therefore, a periodic vibration force is generated in the electromagnetic actuator to cause vibration of the rotor and the base. Because the magnitude of force is proportional to the square of the rotational speed [6], the stability of the magnetic bearing system will be seriously damaged when the vibration force reaches a certain degree.

The unbalanced vibration suppression schemes mostly eliminate the same frequency component in the displacement or current signal. Betschon F et al. [7] effectively reduced the current amplitude in magnetic bearing coils by using variable gain control at different speeds. Shi et al. [8] adopted the least mean square (LMS) algorithm to generate equal-gain and anti-phase signals of the same frequency for the feed-forward compensation of same-frequency current. After adding this control strategy to the control loop, vibration force derived from current stiffness with the same frequency is eliminated. Herzog R et al. [9] used a classical notch filter method to suppress unbalanced vibration forces. On this basis, in order to make the closed-loop system stability adjustable, they also proposed a generalized notch filter method. The above literature results show that suppressing the same frequency component of current can significantly reduce the same-frequency vibration force. However, the unbalanced vibration force of the rotor is difficult to eliminate completely due to the displacement negative stiffness force generated by rotor axis deviation [10].

In this regard, considering the direct relation between magnetic flux and force, an unbalanced vibration suppression method based on flux feedback control is proposed in this paper. A generalized notch filter is used to suppress the same frequency component in the magnetic flux signal to achieve complete elimination of unbalance vibration force. To configure the closed-loop pole of system by selecting the parameter of the transmission matrix properly, the sensitivity function of the system is analyzed based on the transfer function of the actual control system. By this way, the stability of the control system in a large rotational speed range can be ensured after adding the generalized notch filter. Finally, the validity of the method is verified by simulation.

II. ESTABLISHMENT OF FLUX FEEDBACK CONTROL SYSTEM

Considering the direction of the electromagnetic force F and the rotor displacement x in the figure, the levitation force of the rotor can be expressed as follow:

$$F=\left[\left(\phi_p+\phi_c\right)^2-\left(\phi_p-\phi_c\right)^2\right]\Big/\mu_0 A_a \tag{1}$$

where ϕ_p and ϕ_c denote bias flux and control flux respectively; A_a is the magnetic pole equivalent cross-sectional area and μ_0 is the space permeability.

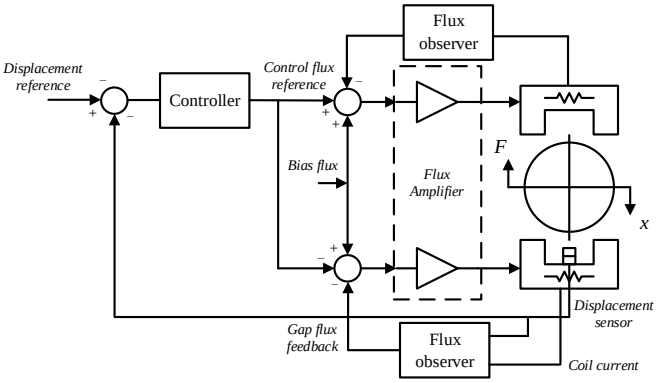

Fig. 1. Block Diagram of Imbalance Compensation Based on Flux Feedback Control

Simplify Eq. (1):

$$F=4\phi_p\phi_c/\mu_0 A_a \tag{2}$$

It can be seen from the above equation that when the bias magnetic flux is a constant value, the levitation force of the flux-controlled magnetic bearing rotor is linearly related to the control magnetic flux. Therefore, the levitation force can be controlled accurately by adjusting the control magnetic flux.

The conventional magnetic bearing control scheme introduces a bias current to linearize the levitation force expression for a linear relationship between the levitation force, the displacement, and the current. This control method does not consider magnetic properties such as magnetic saturation, eddy current, hysteresis, etc. And when the rotor's

displacement fluctuates greatly, the nonlinear relationship between the levitation force, current and displacement makes the performance of the current control scheme disappointing. In the flux control scheme, the control magnetic flux is strictly linear with the levitation force and is independent of the rotor position. Therefore, it can completely eliminate the adverse effects of the above factors in the previous control scheme.

III. Design of Flux Observer

The difficulties in implementing the flux feedback control scheme mainly focus on how to acquire the air gap magnetic flux. Due to the small air gap of the active magnetic bearing, which is usually 0.4*mm*-0.6*mm*, conventional Hall effect sensors are difficult to apply in such applications [11]. Therefore, the observer method is used in this paper to obtain the air gap magnetic flux.

The common flux observer is divided into current model and voltage model [12]. The air gap flux in the current model can be expressed as:

$$\phi_{im} = N\mu_0 A_a i/2s_0 \tag{3}$$

where N is the turns of winding coil， s_0 is the air gap length when the rotor is in an equilibrium position and i is the coil current.

In the Eq. (3), some factors such as magnetic resistance, eddy current, magnetic saturation, and rotor position change of the stator core are neglected. Therefore, this model is accurate only if when the rotor is in a static or low frequency state.

The air gap magnetic flux calculated by the voltage model can be expressed as:

$$\phi_{um} = \int (u - Ri)\,dt \tag{4}$$

where u the winding terminal voltage, R the coil resistance.

The current model is relatively simple but the error is large when the rotor is in a high frequency state due to neglecting the effect of air gap variation on the magnetic flux. The voltage model is more accurate in the high frequency range, but the problem of integral saturation caused by the DC bias in the pure integral link makes the model to be less effective in the low frequency range. Therefore, the current model is modified to fully consider the stator core magnetic circuit, and the rotor real-time position information obtained by the displacement sensor is substituted into the observer model for calculation in this paper.

In order to verify the accuracy of the current model, the air gap flux density was calculated from it in the following eight-pole heteropolar magnetic bearing structure, and the calculated results are compared with the finite element results. The material of the stator and rotor is B20AT1500. The structure of the magnetic bearing is shown in Fig 2.

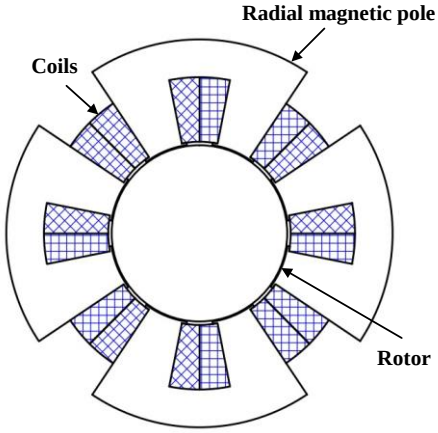

Fig. 2. Radial magnetic bearing section structure

Structural parameters are shown in Table 1:

Table 1. Properties of the AMB.

Property	Value
Rotor radius	35*mm*
Air gap length	0.4*mm*
Inner diameter of pole piece	35.4*mm*
Magnetic pole inner diameter	36.4*mm*
Magnetic pole outside diameter	77*mm*
Magnetic yoke inner diameter	62*mm*
Axial thickness	25*mm*
Pole boots Polar Arc Span	28.5°
Pole/yoke pole arc span	22.5°
B20AT1500 Magnetic permeability	0.0078*H/m*

According to the finite element simulation results, this kind of structural magnetic circuit is simple and there is few magnetic leakage, so the magnetic potential can be considered to be all distributed on ferromagnetic materials and air gaps. Compared to air gaps, the small magnetic reluctance of ferromagnetic materials is neglected in calculations. The air gap flux density can be calculated by the following equation:

$$B_r = Ni/2A_a R_g \tag{5}$$

where R_g represents the magnetoresistance of air gaps. The expressions are as follow:

$$R_g = \left(g_r + (x) \cdot \cos\frac{22.5}{2} \right) \Big/ \mu_0 A_a \tag{6}$$

Where g_r is the air gap length when the rotor is in an equilibrium position and x is the actual displacement of the rotor. And we assume that the down direction is positive.

In the two typical cases where the displacement is fixed in the equilibrium position and the current varies and when the current is fixed in the typical 3A and the displacement varies, the comparison results of magnetic circuit method and finite element method are shown in Figure 3 and Figure 4 respectively.

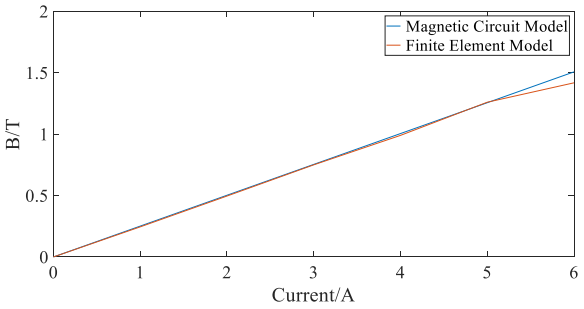

Fig. 3. Rotor displacement is fixed in the equilibrium position and the current varies.

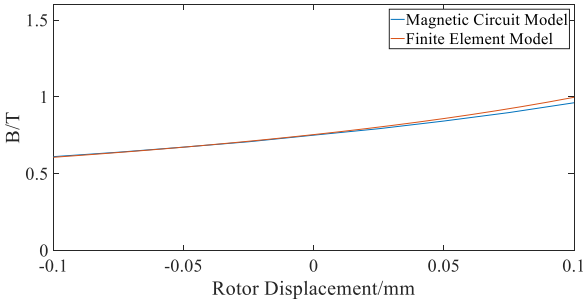

Fig. 4. Coil current is fixed in the typical 3A and the rotor displacement varies.

When the ferromagnetic material is in the magnetized linear region, the error between the magnetic circuit model and the finite element model is quite small. When the coil current exceeds 5A (over the actual operating current range), the non-linear characteristics of the material B-H curve need to be taken into account.

IV. Design and Stability Analysis of Generalized Notch Filter

Compared to the classical notch filter, the generalized notch filter introduces the transfer matrix T so that its poles can be freely configured. The block diagram of the magnetic bearing control system including the generalized notch filter is shown in the Figure. 5:

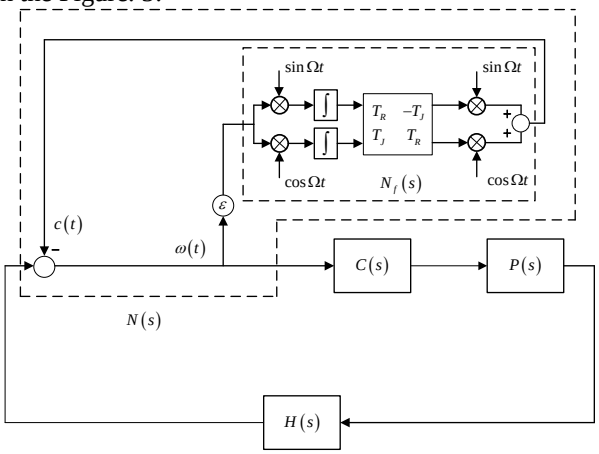

Fig. 5. Block diagram of magnetic bearing system with generalized notch filter

In the figure above, $C(s)$, $P(s)$ and $H(s)$ represents the transfer function of controllers, magnetic bearings and the displacement sensors respectively.

Use $\omega(t)$ and $c(t)$ to denote the open loop input and output signals of the generalized notch filter respectively.

$$c(t)=\begin{bmatrix}\sin(\Omega t) & \cos(\Omega t)\end{bmatrix}\begin{bmatrix}T_R & -T_J\\ T_J & T_R\end{bmatrix}\cdot\int\begin{bmatrix}\sin(\Omega t)\omega(t)\\ \cos(\Omega t)\omega(t)\end{bmatrix}dt \tag{8}$$

Do the following variable substitution:

$$\begin{cases}A=\begin{bmatrix}\sin(\Omega t) & \cos(\Omega t)\end{bmatrix}\\ B=\int\begin{bmatrix}\sin(\Omega t)\omega(t)\\ \cos(\Omega t)\omega(t)\end{bmatrix}dt\\ T=\begin{bmatrix}T_R & -T_J\\ T_J & T_R\end{bmatrix}\end{cases} \tag{9}$$

Substitute (9) into (8) and derivatives on both sides of the equation:

$$\ddot{c}(t)=\ddot{A}TB+2\dot{A}T\dot{B}+AT\ddot{B} \tag{10}$$

After the expansion:

$$\ddot{c}(t)=-\Omega^2c(t)-\Omega T_J\omega(t)+T_R\dot{\omega}(t) \tag{11}$$

Performing Laplace transformation of Eq. (11):

$$s^2C(t)+\Omega^2C(s)=-\Omega T_J\omega(s)+sT_R\omega(s) \tag{12}$$

The open-loop and closed-loop transfer functions of the generalized notch filter are as follows:

$$N_f(s)=\frac{\omega(s)}{C(s)}=\frac{T_Rs-\Omega T_J}{s^2+\Omega^2} \tag{13}$$

$$N(s)=\frac{1}{1+\varepsilon N_f(s)}=\frac{s^2+\Omega^2}{s^2+\varepsilon T_Rs+\Omega^2-\varepsilon\Omega T_J} \tag{14}$$

According to the closed-loop transfer function expression, when the equation satisfies the condition that $\varepsilon\neq 0$ and $\omega=\Omega$, generalized notch filter will attenuate the signal at a specific frequency to zero.

Restate the generalized notch closed-loop transfer function as follows:

$$N(s)=\frac{s^2+\Omega^2}{(s-p)(s-\bar{p})} \tag{15}$$

Consider that:

$$p=j\Omega+re^{j\phi} \tag{16}$$

Substituting equation (16) into equation (15), when $r\ll\Omega$ we can expand the equation to:

$$N(s)=\frac{s^2+\Omega^2}{s^2-2r\cos(\phi)s+\Omega^2+2r\sin(\phi)\Omega} \tag{17}$$

Comparing equations (17) and (14), we can solve that:

$$\begin{cases}\phi=\arg(T_R+jT_J)+\pi\\ r=\dfrac{1}{2}\varepsilon|T_R+jT_J|\end{cases} \tag{18}$$

The closed-loop transfer function poles of the generalized notch filter are shown in Fig. 5.

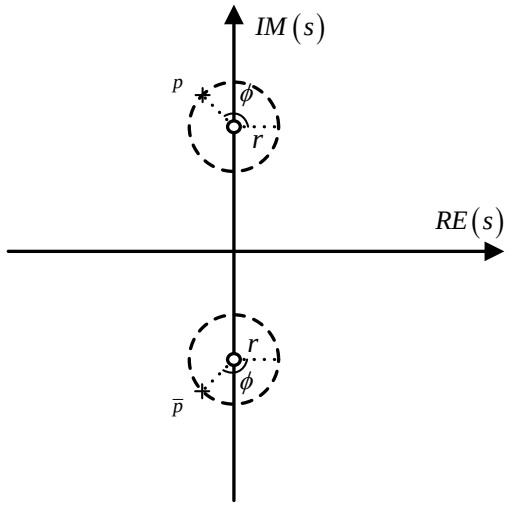

Fig. 6. Pole/zero locations of the generalized notch filter *N*(s).

It can be seen from Eq. (18) and Fig. 6 that compared with the classical notch filter, the generalized notch filter can change the closed-loop pole distribution of the notch filter by adjusting the parameters of the transfer matrix. When the transfer matrix is an identity matrix, the generalized notch filter is identical to the classical notch filter.

Simplified system control block diagram is shown in Fig.7:

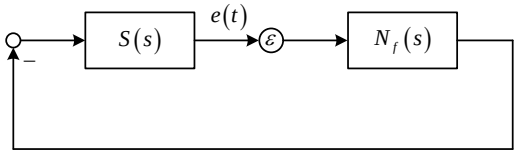

Fig. 7. Simplified system control block diagram.

Where $S(s)$ is the whole system closed-loop sensitivity function and $N_f(s)$ the open loop transfer function of generalized notch filter.

It can be seen from the above figure that the closed-loop eigenvalue of the system after adding the generalized notch filter is the root of the following polynomial:

$$1+\varepsilon N_f(s)S(s)=0 \tag{19}$$

Substituting Eq. (13) into Eq. (19):

$$s^2+\Omega^2+\varepsilon\left(sT_R-\Omega T_J\right)S(s)=0 \tag{20}$$

When the gain is satisfied ε=0 ,the characteristic polynomial has dual characteristic root at $s=j\Omega$ of the imaginary axis. When the gain changes, the eigenvalues will also change. Therefore, the characteristic value is recorded as $s(\varepsilon)$. When the gain approaches 0, We can ensure that the starting angle $\theta=\arg\left[s'(0)\right]$ of the system root locus at the starting point $s=j\Omega$ is within $\left(\frac{\pi}{2},\frac{3\pi}{2}\right)$ by designing a reasonable transfer matrix value. At this point we can guarantee that when the gain satisfies $\varepsilon<\varepsilon'$ (ε' is a certain large gain value) the closed-loop poles of the system are all located in the left half plane, and the system remains stable.

Derivatives on both side of the Eq. (20):

$$\begin{aligned}&2s(\varepsilon)\frac{ds(\varepsilon)}{d\varepsilon}+\left(s(\varepsilon)T_R-\Omega T_J\right)S\left(s(\varepsilon)\right)\\&+\frac{d\left[\left(s(\varepsilon)T_R-\Omega T_J\right)S\left(s(\varepsilon)\right)\right]}{d\varepsilon}\cdot\varepsilon=0\end{aligned} \tag{21}$$

Substituting $\begin{cases}\varepsilon=0\\ s(0)=j\Omega\end{cases}$ into Eq. 21:

$$\left.\frac{\partial s(\varepsilon)}{\partial\varepsilon}\right|_{\varepsilon=0}=s'(0)=-\frac{1}{2}\left(T_R+jT_J\right)S\left(j\Omega\right) \tag{22}$$

From Eq. (22), we can infer that select appropriate transfer matrix parameters based on the system sensitivity function value $S(j\Omega)$, the start angle of the root trajectory θ can be configured. When the transfer function parameter value is satisfied that $\left(T_R+jT_J\right)=S^{-1}(j\Omega)$, The starting angle of the root locus at the imaginary axis is 180° , the closed-loop system can remain stable over a large gain range.

V. Simulation Verification

In the MATLAB/SIMULINK simulation environment, a magnetic suspension control algorithm based on magnetic flux feedback control strategy was built, and a generalized notch filter was added to suppress the same-frequency vibration force.

Prototype simulation parameters are as follows: rotor mass 36*kg*, winding turns 164, winding inductance 16.9*mH* , winding resistance 6Ω ,bias flux 3.063×10^{-4}*wb* , the rotor speed is set to 18000*rpm*.

Respectively, we add generalized notch filter to the current control scheme (A) and flux control scheme (B) two cases. The simulation results are shown as Fig. 8 to Fig.10.

Fig. 8 represents AMB air gap, Fig. 9 represents winding current and gap flux, and Fig. 10 represents magnetic force. Taking into account the gravity of the rotor itself, Fig. 9 shows that the same frequency component of the controlled quantity can be attenuated to an extremely low level in both current and flux control schemes. However, in the Fig. 10, the synchronous magnetic vibration force fluctuation only convergence down to 8N due to the influence of negative displacement stiffness in current control method.

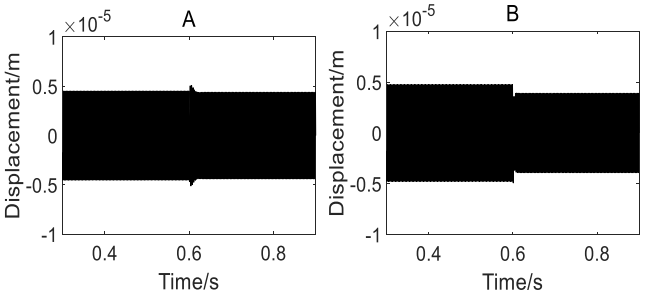

Fig. 8. Actual rotor displacement.

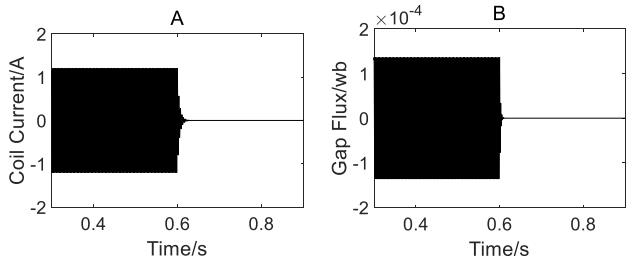

Fig. 9. AMB coil current and gap flux.

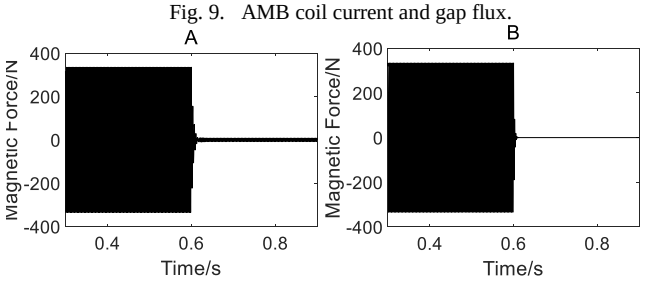

Fig. 10. Magnetic force under two control schemes.

VI. CONCLUSIONS

This paper presents an active vibration control method for magnetic suspension rotor based on flux feedback control. The flux observer was designed according to the parameters of the magnetic bearing, and the results were compared with the finite element simulation results to verify the accuracy of the observer model. The generalized notch filter is used to suppress the same frequency component in the magnetic flux, and the parameters of the notch filter are reasonably designed to ensure the stability of the closed-loop system. Finally, the above work is analyzed and simulated in detail. Compared to the current-mode control method, the suppression of the same frequency in the flux control scheme can completely eliminate the unbalanced vibration force of the rotor.

VII. REFERENCES

[1] Fang J, Ren Y. Decoupling Control of Magnetically Suspended Rotor System in Control Moment Gyros Based on an Inverse System Method[J]. IEEE/ASME Transactions on Mechatronics, 2014, 17(6):1133-1144.

[2] Feng R, Zheng S, Fang J. Online Identification and Unbalanced Vibration Control of High-speed Magnetically Levitated Motor for Drag Test[J]. Journal of Mechanical Engineering, 2014, 50(3):71.

[3] Anselmo J C. Technology Leaps Shape Satellites of Tomorrow[J]. Aviation Week & Space Technology, 1999, 150(4):56-58.

[4] Mohamed A M, Busch-Vishniac I. Imbalance compensation and automation balancing in magnetic bearing systems using the Q-parameterization theory[J]. IEEE Transactions on Control Systems Technology, 1994, 3(2):202-211.

[5] Zheng S, Han B, Feng R, et al. Vibration Suppression Control for AMB-Supported Motor Driveline System Using Synchronous Rotating Frame Transformation[J]. IEEE Transactions on Industrial Electronics, 2015, 62(9):5700-5708.

[6] Schweitzer G, Maslen E H. Magnetic bearings: theory, design, and application to rotating machinery[M]// Magnetic Bearings—Theory, Design and Application to Rotating Machinery. 2009.

[7] Betschon F, Knospe C R. Reducing magnetic bearing currents via gain scheduled adaptive control[J]. IEEE/ASME Transactions on Mechatronics, 2001, 6(4):437-443.

[8] Shi J, Zmood R, Qin L J. The Direct Method for Adaptive Feed-Forward Vibration Control of Magnetic Bearing Systems[J]. European Journal of Dental Education, 2002, 17(1):e142–e150.

[9] Herzog R, Bühler P, Gähler C, et al. Unbalance compensation using generalized notch filters in the multivariable feedback of magnetic bearings[J]. IEEE Transactions on Control Systems Technology, 1996, 45(5):580-586.

[10] Wang Y, Fan Y, Lu M, et al. Micro-vibration control method based on magnetic flux notch filter for magnetically levitated rotor[C]// Control and Decision Conference. IEEE, 2016:3224-3228.

[11] Koseva R, Mönch I, Schumann J, et al. Bismuth Hall probes: Preparation, properties and application[J]. Thin Solid Films, 2010, 518(17):4847-4851.

[12] Zingerli C M, Kolar J W. Novel observer based force control for active magnetic bearings[C]// Power Electronics Conference. IEEE, 2010:2189-2196.